Quantum Electronics **51** (2) 164–168 (2021) © 2021 Kvantovaya Elektronika and IOP Publishing Limited

https://doi.org/10.1070/QEL17431

Simulation on the nonuniform electrical pumping efficiency of THz quantum-cascade lasers

A.K. Dolgov, D.V. Ushakov, A.A. Afonenko, I.N. Dyuzhikov, I.A. Glinskiy, D.S. Ponomarev, R.A. Khabibullin

Abstract. **The efficiency of electric pumping of THz quantum-cascade lasers (QCLs) with strip geometry is studied depending on the number and position of contact pads. The numerical simulation of the electric potential distribution in the THz QCL active region is used to determine the required thicknesses of the upper metallisation layers of the THz QCLs to minimize the voltage drop along the laser structure in the case of nonuniform current supply. It is found that the efficiency of electric pumping in the case of a centrally located contact is significantly higher than when the contact pads are located near the laser structure edges. From the calculated dependence of the THz QCL integral power on the thickness of the upper metal layer, it is shown that for effective current injection, the contact pads must be located at a distance of less than 0.5 mm from each other.**

Keywords: *quantum-cascade lasers, THz range, electric pumping, active region.*

1. Introduction

GaAs/AlGaAs-based quantum-cascade lasers (QCLs) are compact, 1.2 to 5.4 THz, solid-state radiation sources [1, 2], with the frequency range being extended to 10 THz by using HgCdTe mercury compounds [3]. The achieved THz QCL output power of about 1.8 W at the boiling point of liquid nitrogen [4] makes these sources very promising for imaging and probing of distant objects [5, 6]. In addition, the possibility of operating a THz QCL in a cw regime with a lasing spectral width of ~10 kHz [7] allows them to be employed as a local oscillator for heterodyne detection [8], as well as to be used as a source for high-resolution spectroscopy [9–11].

The use of THz QCLs for various applications imposes certain requirements on the laser operation and often determines the active region design and cavity architecture. For example, the use of QCLs in THz imaging systems requires a high output power, improved phase front uniformity, and laser beam asymmetry. In this case, use is made as a rule of active region designs with small values of threshold currents and voltages (for example, the bound-to-continuum design [12]), and a so-called surface plasmon waveguide is employed as a waveguide to improve the far-field radiation pattern. When using a THz QCL as a source for spectroscopy, it is necessary to ensure the laser operation in a single-mode lasing regime with a maximum possible range of radiation frequency tuning [13–15].

Traditionally, two approaches make it possible to implement single-mode lasing in THz QCLs: 1) distributed feedback (DFB) formation [16–18]; 2) two-section coupled Fabry–Perot resonators [18–20]. The DFB in THz QCLs allows suppression of side modes by 20–30 dB and significantly reduces the beam divergence down to 10° [21]. In lasers with two-section coupled Fabry–Perot cavities, side-mode suppression is more than 25 dB, and it becomes possible to tune the laser radiation frequency by about 5 and 12 GHz in cw and pulsed regimes, respectively, by pumping a single cavity section with radiation with a wavelength of ~800 nm [22]. Thus, in both cases, the problem of wire bonding of the THz structure of the QCL laser arises due to a more complex cavity architecture, since the characteristic dimensions required for bonding with a wire ~30 μm in diameter can exceed the dimensions of the topological elements of the waveguide structure. For example, for the implementation of THz QCLs with third-order DFB [23], the contact pad for wire bonding is moved to the periphery, which leads to the single-sided current spreading over the laser structure. When designing surface-emitting THz QCLs, a system of holes in the metal and contact layers is formed on the structure surface for efficient THz radiation output into free space, which leads to the need for wire bonding of free-standing contact pads [24–25]. A similar situation arises in the design of phased THz QCL laser arrays capable of significant improving the radiation efficiency and attain-

A.K. Dolgov, D.S. Ponomarev V.G. Mokerov Institute of Ultra High Frequency Semiconductor Electronics, Russian Academy of Sciences, Nagornyi proezd 7, Stroenie 5, 117105 Moscow, Russia;
D.V. Ushakov, A.A. Afonenko Belarusian State University, prosp. Nezavisimosti 4, 220030 Minsk, Belarus;
I.N. Dyuzhikov Kotel'nikov Institute of Radio Engineering and Electronics, Russian Academy of Sciences, ul. Mokhovaya 11, 125009 Moscow, Russia;
I.A. Glinskiy MIREA – Russian Technological University, prosp. Vernadskogo 78, stroenie 4, 119454 Moscow, Russia;
R.A. Khabibullin V.G. Mokerov Institute of Ultra High Frequency Semiconductor Electronics, Russian Academy of Sciences, Nagornyi proezd 7, Stroenie 5, 117105 Moscow, Russia; Institute for Physics of Microstructures, Russian Academy of Sciences, Division of the Institute of Applied Physics, Russian Academy of Sciences, Akademicheskaya ul. 7, 603087 der. Afonino, Kstovskii raion, Nizhny Novgorod region, Russia;
e-mail: khabibullin@isvch.ru

Received 1 September 2020
Kvantovaya Elektronika **51** (2) 164–168 (2021)
Translated by M.A. Monastyrskiy

ing record-high output powers of more than 2 W, which requires the supply of electric power to the contact pads located in the peripheral part of the laser array [26–27]. This leads to inhomogeneous current injection into the THz QCL active region due to the electrical resistance of the upper cladding of the double metal waveguide, which is traditionally 200–400 nm thick. In addition, the contact pads located at the periphery are limited in area, which allows them to be spliced with one or two wires and, as a result, limits the amount of the current transmitted in such a system.

The aim of this work is to study the electric pumping efficiency of THz QCLs depending on the number and location of contact pads, as well as to determine the required thickness of the upper metal layer in THz QCLs to minimise the voltage drop along the laser structure in the case of inhomogeneous current supply.

2. Simulation of the electric potential distribution in a THz QCL

To evaluate the efficiency of electric pumping of the THz QCL active region, depending on the location of supply wires and on the thickness of the metallisation layer of the waveguide's upper cladding, the electric potential distribution in the laser structure under the application of an external voltage was simulated by the finite element method. For this purpose, a THz QCL model schematically shown in Fig. 1 was constructed in the Comsol Multiphysics software package (Electric Currents module).

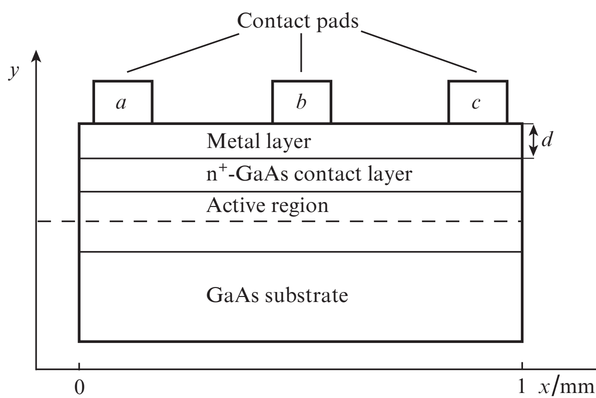

Figure 1. Schematic representation of a THz QCL structure with contact pads. The dashed line indicates the active region cross section used to calculate the electric potential distribution.

The THz QCL model is based on the experimental sample described in [28–31]. This model includes a conductive GaAs substrate with a thickness of 120 μm, an active region based on a $GaAs/Al_{0.15}Ga_{0.85}As$ heterostructure with a thickness of 10 μm, a contact layer n^+-GaAs with a thickness of 100 μm, and a metal layer of gold with a thickness d from 150 to 1900 nm, on which the contact pads are located. The lateral size of the simulated structure corresponds to an experimental THz QCL with a cavity length of 1 mm and a width of 100 μm. The choice of this model's geometry is also due to the fact that the effects of inhomogeneous power supply of a laser strip with a length of 1 mm will only increase with increasing cavity length.

The electric conductivity σ of the layers included in the model was determined as follows. The conductivity of the current-conducting GaAs substrate was calculated as $\sigma_{GaAs} = en\mu_e = 1.6 \times 10^5$ S m^{-1}, where the electron mobility is $\mu_e = 1 \times 10^4$ cm^2 V^{-1} for cryogenic temperatures at a concentration of GaAs doping with silicon $n = 1 \times 10^{18}$ cm^{-3}. The conductivity of the THz QCL active region was estimated based on the resistance $R = 12$ Ohm of the manufactured laser at the operating point, which corresponds to $\sigma = L/(RS) = 8.3$ S m^{-1}, where L is the active region thickness, and S is the cross-sectional area of a rectangular laser strip with a length of 1 mm and a width of 100 μm. Since the contact layer and the conductive substrate are made of the same material, the conductivity of the n^+-GaAs contact layer is equal to the conductivity calculated for the current-conducting GaAs substrate. The conductivity of the metal layer of gold was estimated from the temperature dependence of the resistivity of gold, measured in [32, 33]. At cryogenic temperatures $\rho_{Au} = 1$ μOhm cm, which is equivalent to $\sigma_{Au} = 1/\rho_{Au} = 1 \times 10^8$ S m^{-1}.

To provide power to the simulated laser structure, three contact pads a, b, and c with a lateral size of 50 μm were used (see Fig. 1). To determine the optimal power supply regimes for the active region, the following options were considered: voltage was applied to the contact pad c, contact pad b, contact pads b and c, and contact pads a, b, and c.

The obtained dependences of the electric potential distribution in the THz QCL active region (cross section of the y axis in Fig. 1) were recalculated into the current distributions along the laser strip length. For this purpose, we used the experimental current–voltage characteristic (I–V curve) of a manufactured THz QCL with a resonant-phonon design and a lasing frequency of about 3.3 THz [34].

3. Results and discussion

Figure 2 shows the distributions of the electric potential and current along the laser structure length when a voltage is applied to a single contact area located at the edge (contact area c). When a voltage is applied to the contact c, the electric potential distribution in the THz QCL active region has a decreasing nature. With distance from the contact c, there occurs a voltage drop, which is primarily due to the resistance of the metal layer of gold. At a gold layer thickness $d =$ 150 nm, the voltage drop ΔU on the structure side opposite to the contact c is 2.05 V. This voltage drop corresponds to a drop in the injection current in the active region from 1.76 to 1.58 A, which was determined by the experimental I–V curve of the manufactured THz QCL. In this case, about 50% of the active region area is in the subthreshold injection regime, when the injection current is less than the threshold current $J_{th} = 1.6$ A. Thus, at $d = 150$ nm, the efficiency of electric pumping is low, which leads to a significant decrease in the THz QCL output power.

Figure 2 shows that as the gold layer thickness increases, the voltage drop decreases at the strip edge opposite to the contact c. For example, at $d = 300$, 500, and 850 nm, the voltage drop ΔU is 1, 0.65, and 0.35 V, respectively. If the gold layer thickness exceeds 850 nm, the electric potential is levelled over the entire structure, which corresponds to the case of a uniform THz QCL power supply.

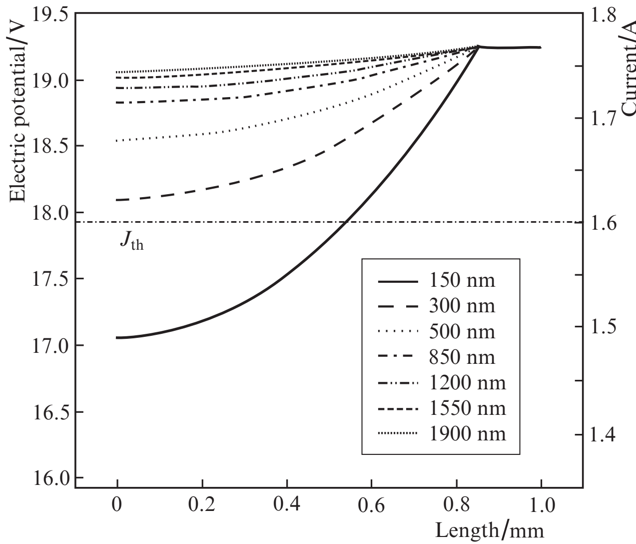

Figure 2. Electric potential and current distributions in a THz QCL with a contact pad located at the structure edge (contact c) at a gold layer thickness from 150 to 1900 nm. The dashed line shows the threshold current value J_{th}.

In the case of applying a voltage to the contact area located in the central region of the structure (contact pad b), the distributions of the electric potential and current in the THz QCL active region are shown in Fig. 3. With a gold layer thickness $d = 150$ nm, the voltage drop ΔU at the edges is 0.6 V, which is equivalent to an injection current drop of 80 mA. An increase in d results in a decrease in ΔU, which for $d > 500$ nm is less than 0.1 V. In this case, for all studied values of d, the injection current exceeds the threshold current $J_{th} = 1.6$ A for the entire active area. Thus, if the contact pad is located at the centre, the efficiency of electric pumping is much higher compared to the case when the contact pad is located at the laser strip edge.

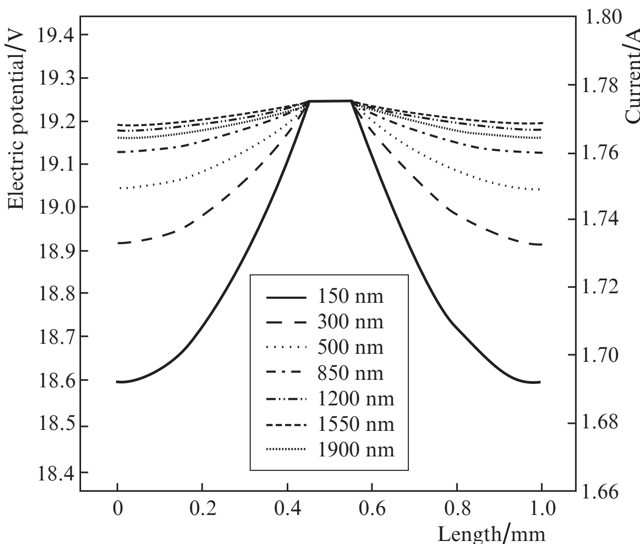

Figure 3. Electric potential and current distributions in a THz QCL with a contact pad in the central region (contact b) at a gold layer thickness from 150 to 1900 nm.

The distribution of the electric potential and current along the structure shown in Fig. 4 corresponds to the case when the voltage is applied to two contact pads located at the centre and close to the laser structure edge (pads b and c). It can be seen that a region with a small voltage drop of less than 0.1 V is formed between the two contacts. In this case, as in the case of a single contact area b, a voltage drop of $\Delta U = 0.6$ V occurs at $d = 150$ nm at the opposite laser strip edge. This approach can be used in the design of high-power lasers to reduce the thermal load of the emitting end-face. By choosing the distance between the contact b and the emitting end-face, and also varying the metallisation layer thickness, it is possible to achieve a significant decrease in the current density in the emitting end-face region and, consequently, to reduce the Joule heating of this region.

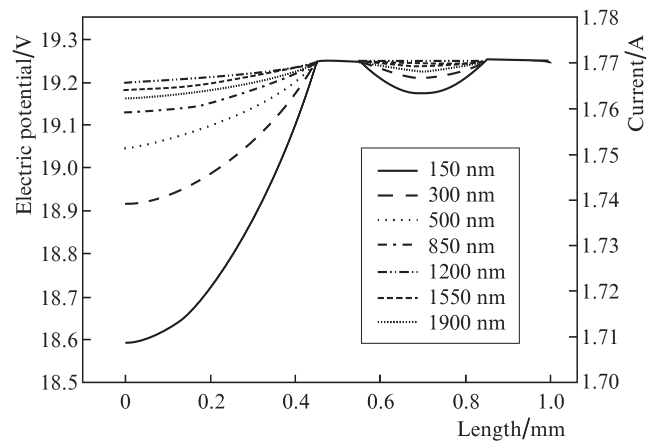

Figure 4. Electric potential and current distributions in a THz QCL with two contact pads b and c at a gold layer thickness from 150 to 1900 nm.

For comparison with the above-described cases of nonuniform supply of THz QCLs, Fig. 5 shows the distributions of the electric potential and current along the laser structure length in the case of voltage supply to three contact pads located at the edges and at the centre of the structure (contact pads a, c, and b). When a voltage is applied to three contact pads, a small voltage drop is observed in the active region between the contact pads, which approximately corresponds to the case of a uniform supply of a THz QCL with the highest efficiency of electric pumping. These calculations clearly demonstrate that the use of contact pads periodically located on the structure's surface can lead to an elaborated modulation of the current injection and, as a consequence, gain modulation in the THz QCL active region. To increase the modulation depth of the current injection, it is necessary to electrically isolate the contact pads from each other, which will require etching the metallisation layer and the n^+-GaAs contact layer.

To assess the effect of the nonuniformity of the electric power supply on the THz QCL output power, the integral power dependence on the gold layer thickness d was plotted for the above-considered cases of the location of contact pads. To this end, we used the experimental dependence of the integral power P on the bias voltage (see the inset in Fig. 6), which allowed us to estimate the effect of the voltage drop ΔU on the P value.

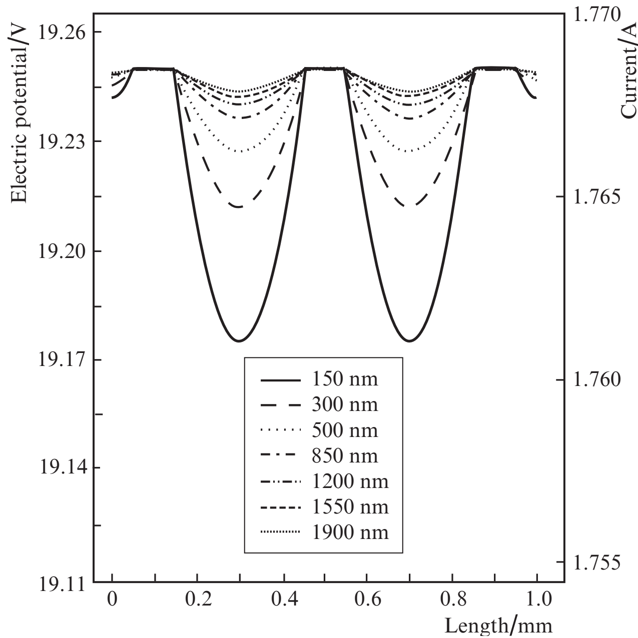

Figure 5. Electric potential and current distributions in a THz QCL with three contact pads a, b, and c at a gold layer thickness from 150 to 1900 nm.

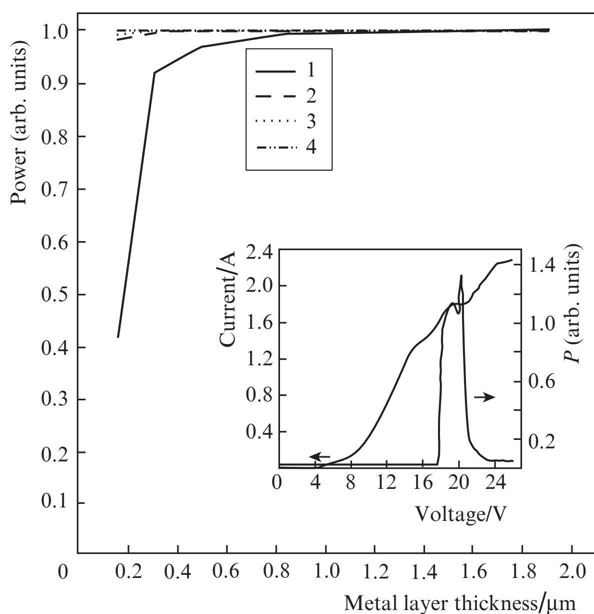

Figure 6. Dependence of the integral power on the upper metallisation layer thickness for four variants of the location of contact pads: 1 = contact pad c; 2 = contact pad b; 3 = two contact pads b and c; 4 = three pads a, b, and c. The inset shows the $I-V$ curve and the dependence of the integral power on the bias voltage for the fabricated THz QCL at 4.2 K.

It can be seen from Fig. 6 that when the contact pad is located at the structure edge (contact pad c) and a thin gold layer (d = 150 nm) is used, a sharp drop in the integral power is observed compared to with the case of a uniform power supply. The voltage drop along the laser structure reduces the output power by 50%–60% at a metallisation layer thickness of 150–200 nm. To increase the efficiency of electric pumping, it is necessary to increase the thickness d to 850 nm or more, which will lead to a small (less than 5%) decrease in the output power compared to the case of a uniform electric supply. It should be noted that the use of a metallisation thickness of more than 850 nm requires additional technological operations (for example, galvanic deposition of gold), which complicates the THz QCL fabrication, taking into consideration the large depth of mesa-etching, about 10 μm of comb-like mesa-stripes [35–37]. However, our calculations show that with a metallisation thickness of about 500 nm, which can be obtained using traditional lift-off lithography, the output power drop is insignificant and amounts to less than 10%. In addition, it follows from Fig. 6 that when using a single contact pad located at the centre (pad b) and three contact pads (pads a, b, and c), the output power values for all studied thicknesses d have similar values for the laser structure length of 1 mm. Thus, when the contact pad is placed in the central part of the THz QCL structure, effective current injection at a gold layer thickness exceeding 150 nm occurs at a distance of 0.5 mm from the contact. This parameter can be used to design a THz QCL with a long cavity (2 mm or more); in this case, for electric pumping, the distance between the supply wires on the structure surface should not exceed 0.5 mm.

4. Conclusions

Thus, we have studied the efficiency of electrical pumping of THz QCLs for four variants of the power supply system. When a voltage is applied to a single contact pad located at the laser structure edge, the voltage drop along the 1 mm long waveguide is about 2 V, which leads to a low efficiency of electric pumping and a reduction in the output power by 60% at an upper metal layer thickness of 150 nm. When a voltage is applied to a single contact pad located at the centre of the laser structure with a length of 1 mm, the efficiency of electric pumping is comparable to that in the case of the voltage supply to two and three contact pads. Thus, if the THz QCL contact pad is located in the peripheral part of the device, then, for efficient electric pumping, it is necessary to use upper metal layers with a thickness of more than 850 nm. If the layer thickness is less than 500 nm and the contact pads are located in the central region of the structure, effective current injection requires the contact pads to be located at a distance of less than 0.5 mm from each other.

Acknowledgements. This work was supported by the Russian Science Foundation (Grant No. 18-19-00493).

References

1. Walther C., Fischer M., Scalari G., et al. *Appl. Phys. Lett.*, **91** (13), 131122 (2007).
2. Wienold M., Röben B., Lü X., et al. *Appl. Phys. Lett.*, **107** (20), 202101 (2015).
3. Ushakov D., Afonenko A., Khabibullin R., et al. *Opt. Express*, **28** (17), 25371 (2020).
4. Li L.H., Chen L., Freeman J.R., et al. *Electron. Lett.*, **53** (12), 799 (2017).
5. Sterczewski L.A., Westberg J., Yang Y., et al. *J. Opt. Soc. Am.*, **6** (6), 766 (2019).
6. Lim Y.L., Bertling K., Taimre T., et al. *Opt. Express*, **27** (7), 10221 (2019).
7. Barkan A., Tittel F.K., Mittleman D.M., et al. *Opt. Lett.*, **29** (6), 575 (2004).
8. Ren Y., Hayton D.J., Hovenier J.N., et al. *Appl. Phys. Lett.*, **101** (10), 101111 (2012).

9. Hübers H.W., Richter H., Wienold M. *J. Appl. Phys*., **125** (15), 151401 (2019).
10. Alam T., Wienold M., Lu X., et al. *Opt. Express*, **27** (4), 5420 (2019).
11. Roben B., Lu X., Hempel M., et al. *Opt. Express*, **25** (14), 16282 (2017).
12. Faist J., Beck M., Aellen T., et al. *Appl. Phys. Lett*., **78** (2), 147 (2001).
13. Lee A.W.M., Williams B.S., Kumar S., et al. *Opt. Lett*., **35** (7), 910 (2010).
14. Kundu I., Dean P., Valavanis A., et al. *ACS Photonics.*, **5** (7), 2912 (2018).
15. Hempel M., Röben B., Schrottke L., et al. *Appl. Phys. Lett*., **108** (19), 191106 (2016).
16. Williams B.S., Kumar S., Hu Q., et al. *Opt. Lett*., **30** (21), 2909 (2005).
17. Wienold M., Tahraoui A., Schrottke L., et al. *Opt. Express*, **20** (10), 11207 (2012).
18. Kumar S., Williams B.S., Qin Q., et al. *Opt. Express*, **15** (1), 113 (2007).
19. Höfling S., Heinrich J., Reithmaier J.P., et al. *Appl. Phys. Lett.*, **89** (24), 241126 (2006).
20. Li H., Manceau J.M., Andronico A., et al. *Appl. Phys. Lett*., **104** (24), 241102 (2014).
21. Biasco S., Garrasi K., Castellano F., et al. *Nat. Commun*., **9**, 1122 (2018).
22. Hempel M., Röben B., Niehle M., et al. *AIP Advances*, **7** (5), 055201 (2017).
23. Wienold M., Röben B., Schrottke L., et al. *Opt. Express.*, **22** (3), 3334 (2014).
24. Jin Y., Gao L., Chen J., et al. *Nat. Commun*., **9**, 1407 (2018).
25. Liang Y., Wang Z., Wolf J., et al. *Appl. Phys. Lett*., **114** (3), 031102 (2019).
26. Jin Y., Reno J.L., Kumar S. *Optica*, **7**, 708 (2020).
27. Jin Y., Zhu O., Reno J.L., Kumar S. *Appl. Phys. Lett.*, **116**, 131103 (2020).
28. Khabibullin R.A., Shchavruk N.V., Ponomarev D.S., et al. *Semiconductors*, **52** (11), 1380 (2018) [*Fiz. Tekh. Poluprovodn*., **52** (11), 1268 (2018)].
29. Khabibullin R.A., Shchavruk N.V., Klochkov A.N., et al. *Semiconductors*, **51** (4), 514 (2016) [*Fiz. Tekh. Poluprovodn*., **51** (4), 540 (2016)].
30. Glinskii I.A., Zenchenko N.V., Maltsev P.P. *Ross. Tekh. Zh*., **4** (3), 27 (2016).
31. Volkov O.Yu., Dyuzhikov I.N., Logunov M.V., et al. *J. Commun. Technol. Electron*., **63** (9), 1042 (2018) [*Radiotekh. Elektron*., **63** (9), 981 (2018)].
32. Ushakov D.V., Afonenko A.A., Dubinov A.A., et al. *Quantum Electron*., **48** (11), 1005 (2018) [*Kvantovaya Elektron*., **48** (11), 1005 (2018)].
33. Khabibullin R., Ushakov D., Afonenko A., et al. *Proc. SPIE*, **11066**, 1106613 (2018).
34. Ushakov D.V., Afonenko A.A., Dubinov A.A., et al. *Quantum Electron*., **49** (10), 913 (2019) [*Kvantovaya Elektron*., **49** (10), 913 (2019)].
35. Khabibullin R.A., Shchavruk N.V., Pavlov A.Yu., et al. *Semiconductors*, **50** (10), 1377 (2016) [*Fiz. Tekh. Poluprovodn*., **50** (10), 1377 (2016)].
36. Ikonnikov A.V., Marem'yanin K.V., Morozov S.V., et al. *Tech. Phys. Lett*., **43** (4), 362 (2016) [*Pis'ma Zh. Tekh. Fiz*., **43** (4), 362 (2016)].
37. Khabibullin R., Ushakov D., Afonenko A., et al. *Proc. SPIE*, **11022**, 1102204 (2019).